Nanostructured GaAs/(Al,Ga)As Waveguide for Low-Density Polariton Condensation from a Bound State in the Continuum

F. Riminucci,[1,2] V. Ardizzone,[3] L. Francaviglia ,[1] M. Lorenzon,[1] C. Stavrakas,[1] S. Dhuey,[1]
A. Schwartzberg,[1] S. Zanotti,[4] D. Gerace,[4] K. Baldwin,[5] L. N. Pfeiffer,[5] G. Gigli,[2,3] D. F. Ogletree ,[1]
A. Weber-Bargioni,[1] S. Cabrini,[1] and D. Sanvitto[3,*]

[1]*Molecular Foundry, Lawrence Berkeley National Laboratory, One Cyclotron Road, Berkeley, California 94720, USA*
[2]*Dipartimento di Matematica e Fisica, "Ennio de Giorgi", Università del Salento, Lecce, Italy*
[3]*CNR Nanotec, Institute of Nanotechnology, via Monteroni, 73100 Lecce, Italy*
[4]*Dipartimento di Fisica, Università di Pavia, via Bassi 6, Pavia, Italy*
[5]*PRISM, Princeton Institute for the Science and Technology of Materials, Princeton University, Princeton, New Jersey 08540, USA*

Exciton-polaritons are hybrid light-matter states that arise from strong coupling between an exciton resonance and a photonic cavity mode. As bosonic excitations, they can undergo a phase transition to a condensed state that can emit coherent light without a population inversion. This aspect makes them good candidates for thresholdless lasers, yet short exciton-polariton lifetime has made it difficult to achieve condensation at very low power densities. In this sense, long-lived symmetry-protected states are excellent candidates to overcome the limitations that arise from the finite mirror reflectivity of monolithic microcavities. In this work we use a photonic symmetry-protected bound state in the continuum coupled to an excitonic resonance to achieve state-of-the-art polariton condensation threshold in a GaAs/(Al, Ga)As waveguide. Most important, we show the influence of fabrication control and how surface passivation via atomic layer deposition provides a way to reduce exciton quenching at the grating sidewalls.

I. INTRODUCTION

Efficient low-threshold lasing is a long-sought goal for various applications spanning from integrated circuits to biological sensing [1,2]. However, to date the emission of coherent and monochromatic light has relied on population inversion, which requires overcoming a threshold excitation power to achieve lasing. A different approach exploits hybrid light-matter particles, known as exciton-polaritons [3,4], which arise in a semiconductor when the energy exchange rate between a photon and an exciton is higher than their losses. These particles possess properties inherited from their photonic component, such as a small effective mass, and from their excitonic component, such as high nonlinearities [5,6] that can be further enhanced via dipolar interactions [7,8]. All these properties make them interesting candidates for devices [9] such as optical transistors [10,11], fast optical switches [12,13], and electrically injected light sources [14].

Because of their bosonic nature, they can undergo a phase transition to a coherent state, known as a Bose-Einstein condensate (BEC) [15,16], without the need for population inversion, making thresholdless lasing theoretically possible [17]. A necessary condition for this phase transition to happen is that the rate of scattering processes [18] that populate the BEC state must exceed the loss rates [9]. This has been one of the main limitations in the historical achievement of exciton-polariton condensates, as polaritons tend to accumulate in the so-called "bottleneck" [19,20]. Such limitation is overcome by growing highly reflective mirrors with layers exceeding 40 pairs in both sides of a microcavity as well as using many stacks of quantum wells (QWs). In the last few years a different approach has enabled the achievement of polariton states in horizontal platforms [5,21–25], making the fabrication easier and less time consuming. A similar waveguide configuration with multiple QWs was used to investigate the enhancement of dipolar polariton interactions [8,26–28]. More recently, the same heterostructure led to the achievement of a Bose-Einstein condensate from a bound state in the continuum (BIC) [29] while also proving the topological charge possessed by the condensate.

In this work we show the achievement of a low-density condensate in a GaAs/(Al, Ga)As waveguide by tuning the

---

parameters of a low-loss shallow grating and then we consider the effect of the reduction of excitonic losses on the threshold. In order to reduce the radiative losses we make use of a topologically protected bound state in the continuum [30–32], which is introduced in the polariton dispersion through the realization of a one-dimensional (1D) etched grating [33]. Since the BIC has an antisymmetric profile, it cannot couple to outgoing plane waves, resulting in a perfectly dark state with zero radiative linewidth [34]. The exciton-polariton dispersion can be modified by changing the grating periodicity, which defines the energy at which the photonic modes cross. Such crossing can then be adjusted to bring the BIC closer to or further from the exciton, changing its excitonic fraction. This will ultimately change the threshold as the excitonic fraction has also an effect on the polariton thermalization towards the BIC. This control is something that has no counterparts in classical vertical microcavities and can be tuned with extreme precision on several different gratings on the same chip. The excitonic fractions are estimated throughout this work by using the coupled oscillators model described in the Supplemental Material [35].

A horizontal configuration and such a long-lived state can drastically ease the fabrication with respect to vertical microcavities in order to achieve thermalization of polaritons into a single quantum state. Here we demonstrate the achievement of low-threshold condensate as a result of simple, yet extremely effective sample processing. We consider three different shallow etched 1D gratings: 40-, 90-, and 130-nm-deep grooves. Finally, we show the reduction of the exciton-polariton linewidth and condensate threshold by passivating the trap states that form on the groove sidewalls during the etching process.

II. RESULTS

The sample is composed of a GaAs substrate on which a waveguide slab is grown via molecular beam epitaxy. $Al_{0.8}Ga_{0.2}As$ (500 nm) is firstly grown onto the substrate, forming the waveguide cladding. A set of 12 GaAs QWs and 13 $Al_{0.4}Ga_{0.6}As$ barriers of 20 nm in thickness are grown on top of the cladding, forming the waveguide core. Lastly, 10 nm of GaAs is grown on top of the last barrier to act as a cap layer. The optical mode is confined in the waveguide core through total internal reflection, and here it exchanges energy with the QW excitons leading to propagating polaritons. A shallow etched 1D grating [Fig. 1(a)] can be used to couple propagating and counter-propagating photonic modes via the slab refractive index modulation; hence, we can easily introduce new properties by engineering the photonic dispersion. In our system we can exploit such coupling between photonic modes to introduce a symmetry-protected bound state in the continuum, which appears in the so-called dark state. If we consider E_{Bright} and E_{Dark} as the photonic modes originating from the grating coupling and separated by an energy gap, the energy exchange with the QW excitons can lead to the following system Hamiltonian:

$$H = \begin{pmatrix} E_{Bright} & \frac{\Omega}{2} & 0 & 0 \\ \frac{\Omega}{2} & X & 0 & 0 \\ 0 & 0 & E_{Dark} & \frac{\Omega}{2} \\ 0 & 0 & \frac{\Omega}{2} & X \end{pmatrix}. \quad (1)$$

The photonic bright and dark states are then hybridized with the exciton, and hence the diagonalization leads to exciton-polariton eigenstates with a BIC in the dark lower
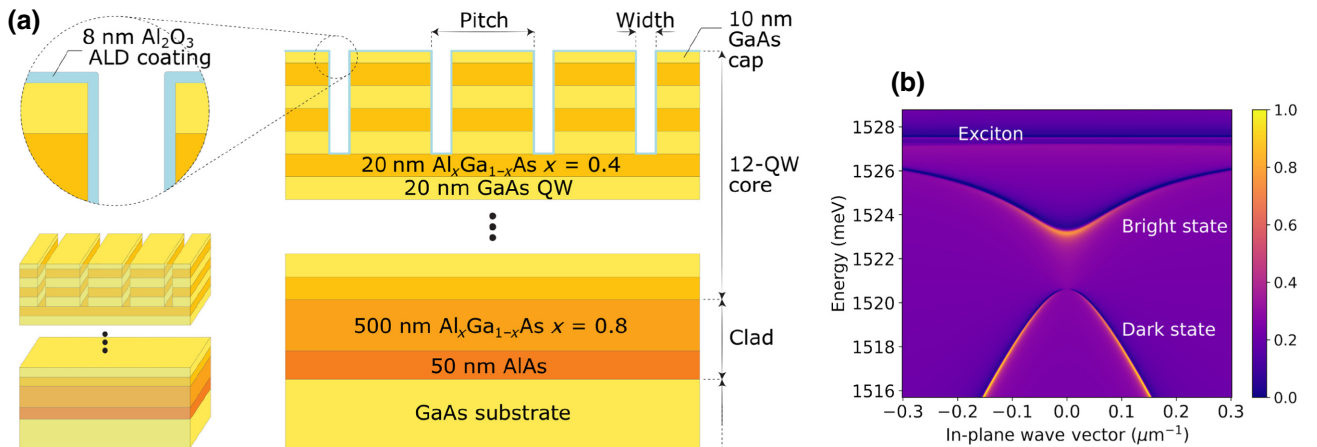

FIG. 1. (a) Sketch of the final processed waveguide sample with a 90-nm-deep grating, along with a conformal passivating layer of Al_2O_3. (b) Simulations of the exciton-polariton dispersion with bright and dark states coupled to the exciton. The BIC appears here as a dark state at the maximum energy point of the dispersion, corresponding to vertical emission ($k_\parallel = 0$) in the far field.

state [Fig. 1(b)] [36]. Since the gap depends on the coupling strength between the photonic modes, it also depends on the grating's fabrication parameters, such as the etching depth and the filling factor, defined as FF = 1 − width/pitch [Fig. 1(a)]. We use Stanford Stratified Structure Solver (S4) [37] to simulate the structure in Fig. 1(a), from which we obtain the energy dispersion shown in Fig. 1(b). The exciton is introduced in the simulations with a Lorentzian resonance in the GaAs dielectric constant, with a Rabi splitting $\Omega = 13.9$ meV [8]. The bound state in the continuum appears as a saddle point of the dark state as shown in Ref. [29], which creates a direct path for polaritons to thermalize from the exciton reservoir.

The fabricated gratings are 50-μm wide and 300-μm long with a filling factor of 70%–75%. The periodicity is set around 240 nm to have the photonic mode coupling close to the exciton resonance. We realize the grooves by writing an electron-beam-sensitive resist, and subsequent pattern transfer into the heterostructure via inductively coupled plasma-chlorine etching [38–41]. The etched grating penetrates into the waveguide core, and three different depths are chosen, resulting in different degrees of photonic coupling.

The sample is cooled down to 4 K in a cryostat and polaritons are created by nonresonantly pumping with a laser onto the grating (see Sec. IV). Light is outcoupled by the grating itself and the energy dispersion imaged on a CCD camera. Accumulation of polaritons in the long-lived state triggers the onset of a coherent emission by bosonic stimulation. The polariton energy dispersion at and above threshold for a grating with FF = 75% is shown in Figs. 2(a) and 2(b).

The power at which the condensation occurs is found to be strongly dependent on the grating parameters. Figure 3 shows the threshold intensity in a 90-nm-deep grating as a function of the periodicity. We choose gratings with periodicities equal to 240, 242, and 244 nm, which correspond to excitonic fractions 51.2%, 22.6%, and 12.1%, respectively. We observe a lower threshold for the 240-nm pitch
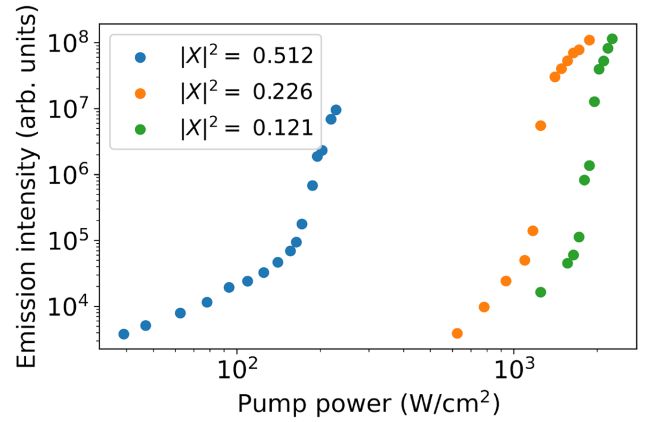

FIG. 3. Emission intensity from the condensate for periodicities of 240 nm (blue), 242 nm (orange), and 244 nm (green). The excitonic fraction $|X|^2$ is modified by the grating pitch, favoring a polariton thermalization towards the BIC and reducing the power threshold in the 240-nm case.

with respect to the 242- and 244-nm cases, ascribable to the higher exciton fraction. In our system, the grating periodicity moves the BIC closer to or further from the exciton, making the polariton thermalization process more or less efficient for the two cases.

In order to reduce the threshold, different etching depths d are studied with filling factors close to 70%, namely 40, 90, and 130 nm, and the measured dispersions are reported in Fig. S6d-f within the Supplemental Material [35]. The etching is performed in the waveguide core, which has consequences for the quality of the polariton modes. The trap states in the electronic band gap created during the fabrication lead to nonradiative exciton surface recombination at the QW sidewalls. Surface recombination can be minimized through oxide removal and surface passivation, achievable through etching at sufficiently low ion energy to remain in the ion-assisted chemical etching regime [42–44]. For this reason, the sample is immersed in a hydrochloric acid bath to remove the surface oxide,
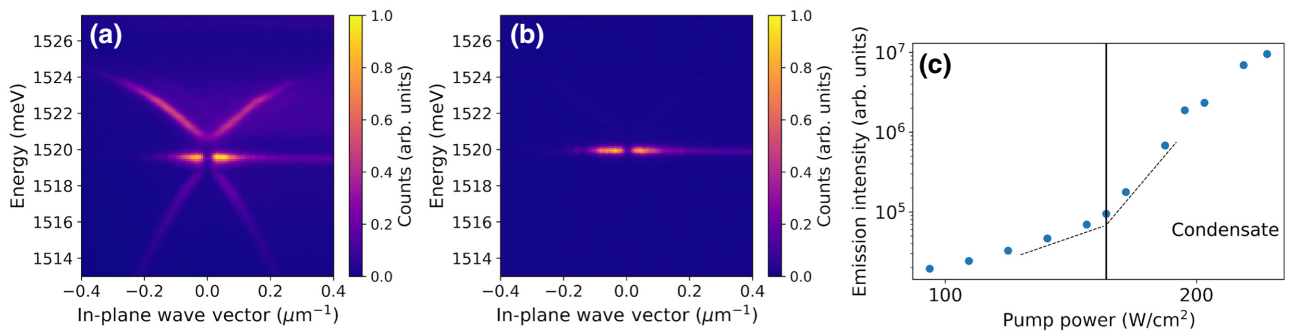

FIG. 2. Exciton-polariton energy dispersion and coherent light emission at (a) and above (b) the excitation threshold. The condensate in (b) is blue-shifted as a result of polariton-polariton interactions. (c) Emission intensity from the condensate as a function of the pumping power.
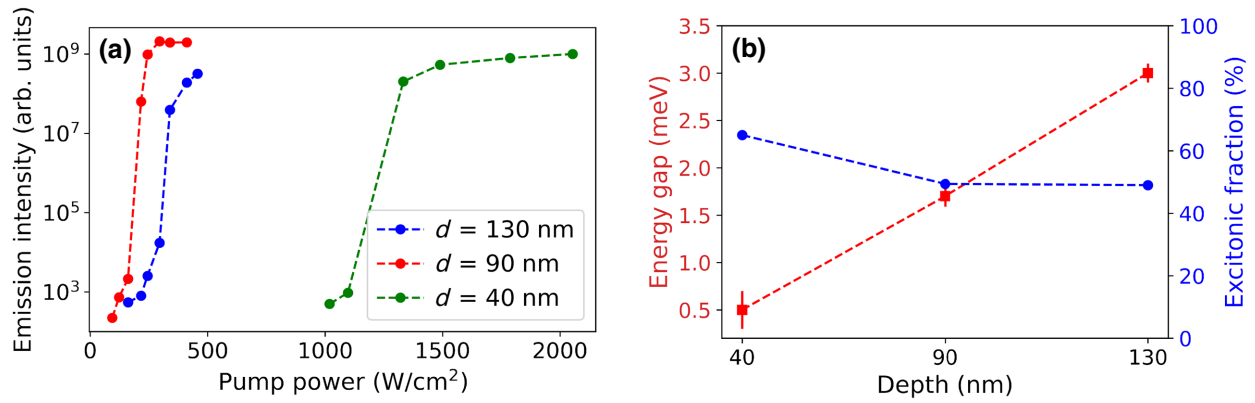
FIG. 4. (a) Emission intensity as a function of the pump power. The threshold is minimum for a grating 90-nm deep, while it is higher for a 40-nm-deep grating due to smaller gap size, and for a 130-nm-deep grating due to surface damage. (b) Energy gap and excitonic fraction as a function of the etching depth. The filling factor is approximately the same in all three cases.

and then 8 nm of Al_2O_3 is deposited via atomic layer deposition (ALD) [45–48] at 300 °C [49]. The observed intensity emissions in the three cases along with the gap size and excitonic fraction are shown in Figs. 4(a) and 4(b).

The lower threshold observed in deeper gratings is caused by a larger gap. In fact, the BIC is more protected from the lossy bright state when the gap is larger. In other words, the smaller the gap, the closer the BIC is to the bright state, and
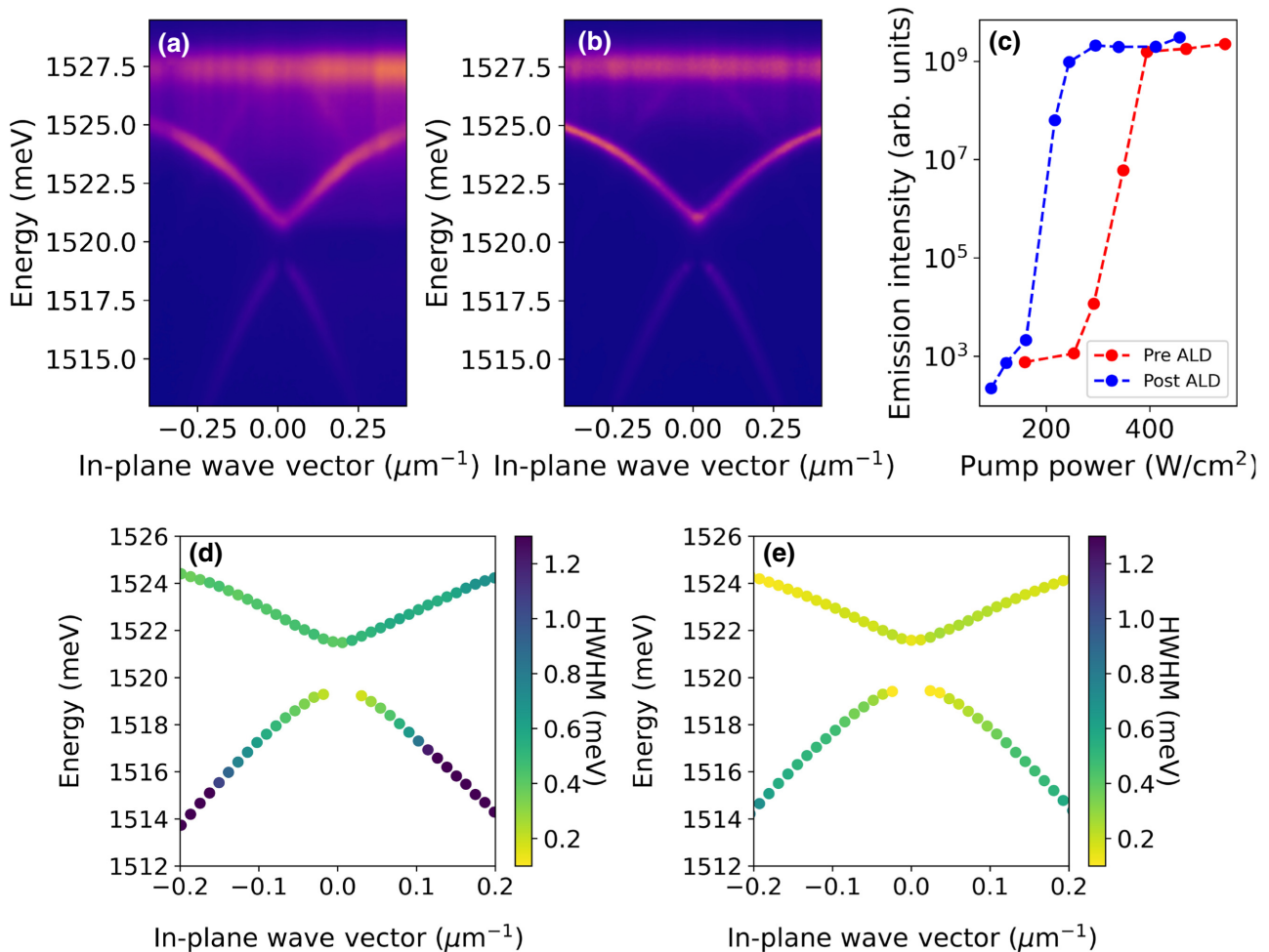

FIG. 5. Exciton-polariton energy dispersion (a) pre-processing and (b) post-processing. (c) Lasing intensity measured at the threshold before and after aluminum oxide deposition for a 90-nm-deep grating, 240-nm pitch. (d),(e) Exciton-polariton dispersions corresponding to (a),(b). Colors represent the HWHM fit of the linewidths.

the higher the losses induced by leakage of the polariton population into the lossy state. Concurrently with the etching depth, the surface damage increases as demonstrated by the 130-nm-deep grating in which the condensate is achieved only from one structure with a high filling factor, and only after post-processing, as a consequence of a more pronounced damage (see Fig. S11 within the Supplemental Material [35]). The damage induced by the etching is found to act mainly on the excitonic component, as shown in Fig. 5 and it is discussed in the Supplemental Material [35] where cathodoluminescence hyperspectral maps elucidate the effect of surface damage on the emission [50–52].

Lastly we observe the effect of post-processing on gratings characterized by 240-nm pitch and 90-nm-deep grooves before and after passivation. The polariton dispersion for this grating is shown in Figs. 5(a) and 5(b), where the threshold reaches an energy per pulse corresponding to a few μJ/cm^2 after ALD as displayed in Fig. 5(c). This measurement is performed on several gratings, and all of them show the same characteristic reduction (see Fig. S10 within the Supplemental Material [35]). The longer polariton lifetime, which we associate with lower nonradiative exciton recombination at the groove sidewalls, can be observed in terms of linewidth reduction after Al$_2$O$_3$ deposition [Fig. 5(e)]. This result, even though limited by the spectrometer resolution and inhomogeneous broadening, clearly highlights the reduction of exciton inhomogeneous broadening, which ultimately corresponds to a longer exciton-polariton lifetime. A more detailed discussion about the BIC lifetime is presented in Ref. [29] where a lower limit is set by means of polariton propagation under the grating. While the effect on the excitonic component is clear, no significant shift in the polariton dispersion is observed after the aluminum oxide deposition, a sign that the lower Al$_2$O$_3$ refractive index ($n = 1.6$ for thin film) compared with the photonic mode effective refractive index ($n = 3.359$) does not alter the designed structure behavior.

III. CONCLUSIONS

The main limitation in achieving thresholdless exciton-polariton lasing is represented by nonradiative and radiative losses that are inevitably present in microcavities. In this work we realize a low-density exciton-polariton condensate in a horizontal cavity that makes use of the long lifetime of a quasibound state in the continuum, the lifetime of which is increased by several orders of magnitude due to the special nature of this dark state. However, surface damage during processing introduces nonradiative channels through which excitons can decay. By performing surface ALD post-processing we greatly reduce such an effect, increasing the polariton lifetime at the BIC. Our method substantially lowers the power needed to achieve

a polariton condensate. This system is not only a good candidate for low-threshold lasers, but also for those experiments that are affected by the simultaneous presence of horizontal and vertical polariton lasing as recently reported in Ref. [22]. In conclusion we assess the role of grating parameters and fabrication in the achievement of state-of-the-art polariton BEC arising from a bound state in the continuum coupled to an excitonic resonance. The extremely long lifetime of the polariton BIC facilitates the thermalization of the bosonic gas with the onset for condensation at a low polariton density despite the presence of lower-energy states. Finally we also observe the reduction of the threshold and improvement in the polariton lifetime after hydrochloric acid treatment and passivation of the sidewalls via atomic layer deposition, reducing the density of nonradiative recombination centers at the QW sidewalls. In the case of deep etching, the role of ALD is crucial, given it is able to restore the possibility of observing the condensate from one 130-nm-deep grating, while it reduces the threshold in all the 90-nm-deep gratings. The linewidth narrowing observed after post-processing is related to the reduction of nonradiative recombination, improving the overall quality factor of the sample leading to an estimated polariton lifetime of a few hundreds of picoseconds in the BIC [29]. Since BEC formation from a BIC has the great advantage of reaching the phase transition at extremely low densities, it can be used to obtain ultralow-threshold lasers. The techniques and ideas investigated and developed here will not only boost the realization of polariton-based thresholdless lasers, but could also be a way to realize horizontal electrically pumped polariton light sources.

IV. MATERIALS AND METHODS

Optical Measurements. The sample is kept at 4 K for all the experiments. All measurements are performed using a 150-fs, 80-MHz pump laser with its central energy tuned at 1.588 meV (780 nm), and a spot size of 15 μm FWHM. The emission from the sample is sent to a SpectraPro-300i spectrometer with a 1200-lines/mm grating in order to reconstruct the reciprocal space. The optical setup allows the simultaneous acquisition of Fourier-space and real-space images, which makes it possible to keep the sample in focus at all times. To remove spurious effects, the laser tail is cut at around 800 nm by a short pass filter, combined with a spatial filter, which removes any emission outside the selected grating region.

ACKNOWLEDGMENTS

The authors declare no conflicts of interest.

[1] R. M. Ma and R. F. Oulton, Applications of nanolasers, Nat. Nanotechnol. **14,** 12 (2019).

[2] M. T. Hill and M. C. Gather, Advances in small lasers, Nat. Photonics **8,** 908 (2014).

[3] C. Weisbuch, M. Nishioka, A. Ishikawa, and Y. Arakawa, Observation of the Coupled Exciton-Photon Mode Splitting in a Semiconductor Quantum Microcavity, Phys. Rev. Lett. **69,** 3314 (1992).

[4] A. Kavokin, J. J. Baumberg, G. Malpuech, and F. P. Laussy, *Microcavities* (Oxford University Press, 2008), p. 1.

[5] P. M. Walker, C. E. Whittaker, D. V. Skryabin, E. Cancellieri, B. Royall, M. Sich, I. Farrer, D. A. Ritchie, M. S. Skolnick, and D. N. Krizhanovskii, Spatiotemporal continuum generation in polariton waveguides, Light: Sci. Appl. **8,** 6 (2019).

[6] E. Estrecho, T. Gao, N. Bobrovska, D. Comber-Todd, M. D. Fraser, M. Steger, K. West, L. N. Pfeiffer, J. Levinsen, M. M. Parish, T. C. Liew, M. Matuszewski, D. W. Snoke, A. G. Truscott, and E. A. Ostrovskaya, Direct measurement of polariton-polariton interaction strength in the Thomas-Fermi regime of exciton-polariton condensation, Phys. Rev. B **100,** 035306 (2019).

[7] E. Togan, H. T. Lim, S. Faelt, W. Wegscheider, and A. Imamoglu, Enhanced Interactions between Dipolar Polaritons, Phys. Rev. Lett. **121,** 227402 (2018).

[8] D. G. Suárez-Forero, F. Riminucci, V. Ardizzone, N. Karpowicz, E. Maggiolini, G. Macorini, G. Lerario, F. Todisco, M. D. Giorgi, L. Dominici, D. Ballarini, G. Gigli, A. S. Lanotte, K. West, K. Baldwin, L. Pfeiffer, and D. Sanvitto, Enhancement of Parametric Effects in Polariton Waveguides Induced by Dipolar Interactions, Phys. Rev. Lett. **126,** 137401 (2021).

[9] D. Sanvitto and S. Kéna-Cohen, The road towards polaritonic devices, Nat. Mater. **15,** 1061 (2016).

[10] D. Ballarini, M. De Giorgi, E. Cancellieri, R. Houdré, E. Giacobino, R. Cingolani, A. Bramati, G. Gigli, and D. Sanvitto, All-optical polariton transistor, Nat. Commun. **4,** 1778 (2013).

[11] C. Sturm, D. Tanese, H. Nguyen, H. Flayac, E. Galopin, A. Lemaître, I. Sagnes, D. Solnyshkov, A. Amo, G. Malpuech, and J. Bloch, All-optical phase modulation in a cavity-polariton Mach–Zehnder interferometer, Nat. Commun. **5,** 3278 (2014).

[12] A. V. Zasedatelev, A. V. Baranikov, D. Sannikov, D. Urbonas, F. Scafirimuto, V. Y. Shishkov, E. S. Andrianov, Y. E. Lozovik, U. Scherf, T. Stöferle, R. F. Mahrt, and P. G. Lagoudakis, Single-photon nonlinearity at room temperature, Nature **597,** 493 (2021).

[13] D. G. Suárez-Forero, F. Riminucci, V. Ardizzone, A. Gianfrate, F. Todisco, M. De Giorgi, D. Ballarini, G. Gigli, K. Baldwin, L. Pfeiffer, and D. Sanvitto, Ultrafast, low-energy, all-optical switch in polariton waveguides, (2021), ArXiv:2110.05704.

[14] C. Schneider, A. Rahimi-Iman, N. Y. Kim, J. Fischer, I. G. Savenko, M. Amthor, M. Lermer, A. Wolf, L. Worschech, V. D. Kulakovskii, I. A. Shelykh, M. Kamp, S. Reitzenstein, A. Forchel, Y. Yamamoto, and S. Höfling, An electrically pumped polariton laser, Nature **497,** 348 (2013).

[15] J. Kasprzak, M. Richard, S. Kundermann, A. Baas, P. Jeambrun, J. M. Keeling, F. M. Marchetti, M. H. Szymánska, R. André, J. L. Staehli, V. Savona, P. B. Littlewood, B. Deveaud, and L. S. Dang, Bose-Einstein condensation of exciton polaritons, Nature **443,** 409 (2006).

[16] T. Byrnes, N. Y. Kim, and Y. Yamamoto, Exciton-polariton condensates, Nat. Phys. **10,** 803 (2014).

[17] A. Imamoglu, R. J. Ram, S. Pau, and Y. Yamamoto, Nonequilibrium condensates and lasers without inversion: Exciton-polariton lasers, Phys. Rev. A - At., Mol., Opt. Phys. **53,** 4250 (1996).

[18] H. J. Miesner, D. M. Stamper-Kurn, M. R. Andrews, D. S. Durfee, S. Inouye, and W. Ketterle, Bosonic stimulation in the formation of a Bose-Einstein condensate, Science **279,** 1005 (1998).

[19] F. Tassone, C. Piermarocchi, V. Savona, and A. Quattropani, Bottleneck effects in the relaxation and photoluminescence of microcavity polaritons, Phys. Rev. B - Cond. Matter Mater. Phys. **56,** 7554 (1997).

[20] M. Richard, J. Kasprzak, R. André, R. Romestain, L. S. Dang, G. Malpuech, and A. Kavokin, Experimental evidence for nonequilibrium Bose condensation of exciton polaritons, Phys. Rev. B **72,** 201301 (2005).

[21] O. Jamadi, F. Reveret, P. Disseix, F. Medard, J. Leymarie, A. Moreau, D. Solnyshkov, C. Deparis, M. Leroux, E. Cambril, S. Bouchoule, J. Zuniga-Perez, and G. Malpuech, Edge-emitting polariton laser and amplifier based on a ZnO waveguide, Light: Sci. Appl. **7,** 82 (2018).

[22] O. Jamadi, F. Réveret, D. Solnyshkov, P. Disseix, J. Leymarie, L. Mallet-Dida, C. Brimont, T. Guillet, X. Lafosse, S. Bouchoule, F. Semond, M. Leroux, J. Zuniga-Perez, and G. Malpuech, Competition between horizontal and vertical polariton lasing in planar microcavities, Phys. Rev. B **99,** 085304 (2019).

[23] P. M. Walker, L. Tinkler, M. Durska, D. M. Whittaker, I. J. Luxmoore, B. Royall, D. N. Krizhanovskii, M. S. Skolnick, I. Farrer, and D. A. Ritchie, Exciton polaritons in semiconductor waveguides, Appl. Phys. Lett. **102,** 012109 (2013).

[24] D. M. Di Paola, P. M. Walker, R. P. Emmanuele, A. V. Yulin, J. Ciers, Z. Zaidi, J. F. Carlin, N. Grandjean, I. Shelykh, M. S. Skolnick, R. Butté, and D. N. Krizhanovskii, Ultrafast-nonlinear ultraviolet pulse modulation in an AlInGaN polariton waveguide operating up to room temperature, Nat. Commun. **12,** 1 (2021).

[25] D. G. Suárez-Forero, F. Riminucci, V. Ardizzone, M. De Giorgi, L. Dominici, F. Todisco, G. Lerario, L. N. Pfeiffer, G. Gigli, D. Ballarini, and D. Sanvitto, Electrically controlled waveguide polariton laser, Optica **7,** 1579 (2020).

[26] I. Rosenberg, Y. Mazuz-Harpaz, R. Rapaport, K. West, and L. Pfeiffer, Electrically controlled mutual interactions of flying waveguide dipolaritons, Phys. Rev. B **93,** 195151 (2016).

[27] I. Rosenberg, D. Liran, Y. Mazuz-Harpaz, K. West, L. Pfeiffer, and R. Rapaport, Strongly interacting dipolar-polaritons, Sci. Adv. **4,** eaat8880 (2018).

[28] D. Liran, I. Rosenberg, K. West, L. Pfeiffer, and R. Rapaport, Fully guided electrically controlled exciton polaritons, ACS Photonics **5,** 4249 (2018).

[29] V. Ardizzone, F. Riminucci, S. Zanotti, A. Gianfrate, M. Efthymiou-Tsironi, D. G. Suárez-Forero, F. Todisco, M. De Giorgi, D. Trypogeorgos, G. Gigli, K. Baldwin, L. Pfeiffer, D. Ballarini, H. S. Nguyen, D. Gerace, and D. Sanvitto, Polariton Bose–Einstein condensate from a bound state in the continuum, Nature **605,** 447 (2022).

[30] A. Kodigala, T. Lepetit, Q. Gu, B. Bahari, Y. Fainman, and B. Kanté, Lasing action from photonic bound states in continuum, Nature **541,** 196 (2017).

[31] C. W. Hsu, B. Zhen, A. D. Stone, J. D. Joannopoulos, and M. Soljačić, Bound states in the continuum, Nat. Rev. Mater. **1,** 16048 (2016).

[32] H. M. Doeleman, F. Monticone, W. Den Hollander, A. Alù, and A. F. Koenderink, Experimental observation of a polarization vortex at an optical bound state in the continuum, Nat. Photonics **12,** 397 (2018).

[33] V. Kravtsov, E. Khestanova, F. A. Benimetskiy, T. Ivanova, A. K. Samusev, I. S. Sinev, D. Pidgayko, A. M. Mozharov, I. S. Mukhin, M. S. Lozhkin, Y. V. Kapitonov, A. S. Brichkin, V. D. Kulakovskii, I. A. Shelykh, A. I. Tartakovskii, P. M. Walker, M. S. Skolnick, D. N. Krizhanovskii, and I. V. Iorsh, Nonlinear polaritons in a monolayer semiconductor coupled to optical bound states in the continuum, Light: Sci. Appl. **9,** 56 (2020).

[34] B. Zhen, C. W. Hsu, L. Lu, A. D. Stone, and M. Soljačić, Topological Nature of Optical Bound States in the Continuum, Phys. Rev. Lett. **113,** 257401 (2014).

[35] See Supplemental Material at http://link.aps.org/supplemental/10.1103/PhysRevApplied.18.024039 for details regarding the nanofabrication, 2-steps model, S4 simulations, and cathodoluminescence.

[36] L. Lu, Q. Le-Van, L. Ferrier, E. Drouard, C. Seassal, and H. S. Nguyen, Engineering a light–matter strong coupling regime in perovskite-based plasmonic metasurface: quasi-bound state in the continuum and exceptional points, Photon. Res. **8,** A91 (2020).

[37] V. Liu and S. Fan, S 4: A free electromagnetic solver for layered periodic structures, Comput. Phys. Commun. **183,** 2233 (2012).

[38] Z. Liao and J. S. Aitchison, Precision etching for multi-level AlGaAs waveguides, Opt. Mater. Express **7,** 895 (2017).

[39] T. Maeda, J. W. Lee, R. J. Shul, J. Han, J. Hong, E. S. Lambers, S. J. Pearton, C. R. Abernathy, and W. S. Hobson, Inductively coupled plasma etching of III-V semiconductors in BCl_3-based chemistries. I. GaAs, GaN, GaP, GaSb and AlGaAs, Appl. Surf. Sci. **143,** 174 (1999).

[40] X. Zhou, I. Kulkova, T. Lund-Hansen, S. L. Hansen, P. Lodahl, and L. Midolo, High-efficiency shallow-etched grating on GaAs membranes for quantum photonic applications, Appl. Phys. Lett. **113,** 1 (2018).

[41] K. A. Atlasov, P. Gallo, A. Rudra, B. Dwir, and E. Kapon, Effect of sidewall passivation in BCl3/N2 inductively coupled plasma etching of two-dimensional GaAs photonic crystals, J. Vac. Sci. Technol. B: Microelectron. Nanometer Struct. **27,** L21 (2009).

[42] O. J. Glembocki, J. A. Tuchman, K. K. Ko, S. W. Pang, A. Giordana, R. Kaplan, and C. E. Stutz, Effects of electron cyclotron resonance etching on the ambient (100) GaAs surface, Appl. Phys. Lett. **66,** 3054 (1995).

[43] D. Leonhardt, C. R. Eddy, V. A. Shamamian, R. T. Holm, O. J. Glembocki, and J. E. Butler, Surface chemistry and damage in the high density plasma etching of gallium arsenide, J. Vac. Sci. Technol. A: Vac., Surf., Films **16,** 1547 (1998).

[44] C. R. Eddy, O. J. Glembocki, D. Leonhardt, V. A. Shamamian, R. T. Holm, B. D. Thoms, J. E. Butler, and S. W. Pang, Gallium arsenide surface chemistry and surface damage in a chlorine high density plasma etch process, J. Electron. Mater. **26,** 1320 (1997).

[45] B. Guha, F. Marsault, F. Cadiz, L. Morgenroth, V. Ulin, V. Berkovitz, A. Lemaître, C. Gomez, A. Amo, S. Combrié, B. Gérard, G. Leo, and I. Favero, Surface-enhanced gallium arsenide photonic resonator with quality factor of 6×10^6, Optica **4,** 218 (2017).

[46] C. L. Hinkle, A. M. Sonnet, E. M. Vogel, S. McDonnell, G. J. Hughes, M. Milojevic, B. Lee, F. S. Aguirre-Tostado, K. J. Choi, H. C. Kim, J. Kim, and R. M. Wallace, GaAs interfacial self-cleaning by atomic layer deposition, Appl. Phys. Lett. **92,** 071901 (2008).

[47] D. Mikulik, A. C. Meng, A. Berrazouane, J. Stückelberger, P. Romero-Gomez, K. Tang, F. Haug, A. Fontcuberta i Morral, and P. C. McIntyre, Surface defect passivation of silicon micropillars, Adv. Mater. Interfaces **5,** 1800865 (2018).

[48] V. Dhaka, A. Perros, S. Naureen, N. Shahid, H. Jiang, J.-P. Kakko, T. Haggren, E. Kauppinen, A. Srinivasan, and H. Lipsanen, Protective capping and surface passivation of III-V nanowires by atomic layer deposition, AIP Adv. **6,** 015016 (2016).

[49] I. V. Levitskii, M. I. Mitrofanov, G. V. Voznyuk, D. N. Nikolaev, M. N. Mizerov, and V. P. Evtikhiev, Annealing of FIB-induced defects in GaAs/AlGaAs heterostructure, Semiconductors **52,** 1898 (2018).

[50] M. Negri, L. Francaviglia, D. Dumcenco, M. Bosi, D. Kaplan, V. Swaminathan, G. Salviati, A. Kis, F. Fabbri, and A. Fontcuberta I Morral, Quantitative nanoscale absorption mapping: A novel technique to probe optical absorption of two-dimensional materials, Nano Lett. **20,** 567 (2020).

[51] P. Hovington, D. Drouin, and R. Gauvin, CASINO: A new Monte Carlo code in C language for electron beam interaction - Part I: Description of the program, Scanning **19,** 1 (1997).

[52] D. Drouin, A. R. Couture, D. Joly, X. Tastet, V. Aimez, and R. Gauvin, CASINO V2.42 - A fast and easy-to-use modeling tool for scanning electron microscopy and microanalysis users, Scanning **29,** 92 (2007).